Chapter 18
Graphene and Carbon Nanotubes

Abstract The phononic properties and the band structure of graphene and carbon nanotubes of different chirality are given and derived within elementary models. Also inorganic atomic sheets and nanotubes such as BN are briefly discussed.

18.1 Graphene

18.1.1 Structure

Graphene is a single sheet of carbon atoms in hexagonal arrangement (Fig. 18.1). The carbon bond length is $d_{\mathrm{C-C}} = 0.142\,\mathrm{nm}$. It can be prepared from graphite via micromechanical cleavage, i.e. mechanical exfoliation (repeated peeling) of small mesas of highly oriented pyrolytic graphite [1285, 1286]. Graphite is a stacked arrangement of such graphene sheets (Fig. 18.2a) held together by van-der-Waals forces as shown in Fig. 18.2b. The carbon atoms bond in-plane via sp^2 hybridization. Organic molecules such as, e.g., anthracene or coronene (Fig. 17.1) can be understood as molecular-size pieces of such two-dimensional graphene sheet with hydrogen saturating the outside, broken bonds. In literature single layer graphene sheets (SLG) and few-layer graphene (FLG) sheets are distinguished. Ideally such two-dimensional crystal is infinitely extended, e.g. for band structure calculations. Real crystals have a boundary (surface) which is topologically a line or very thin sidewall. The mechanical properties of graphene are discussed in [1287].

The phonon dispersion of graphene is shown in Fig. 18.3. For the ZA and ZO modes the displacement is perpendicular to the graphene plane (out-of plane modes).

18.1.2 Band Structure

A single layer of graphene is a zero-gap semiconductor (cf. Fig. 6.40) which shows a linear photon-like spectrum

$$E = \hbar k\, c_* \tag{18.1}$$

M. Grundmann, *The Physics of Semiconductors*, Graduate Texts in Physics,
DOI 10.1007/978-3-319-23880-7_18

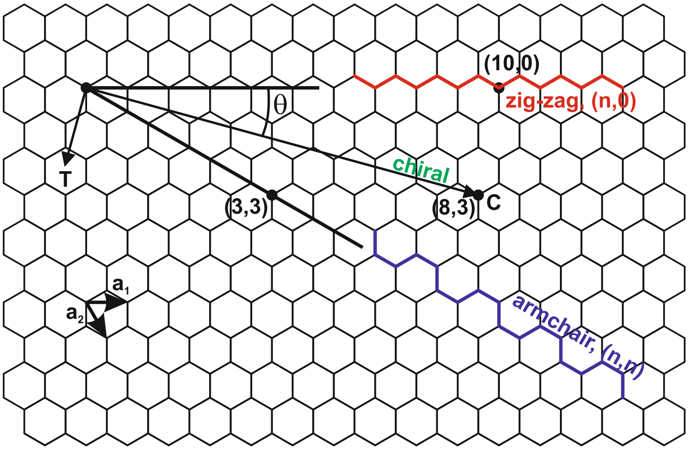

Fig. 18.1 Schematic atomic arrangement in graphene; the C–C bond length is $d_{\mathrm{C-C}} = 0.142\,\mathrm{nm}$. Several vectors for making carbon nanotubes (cf. Sect. 18.2) are shown

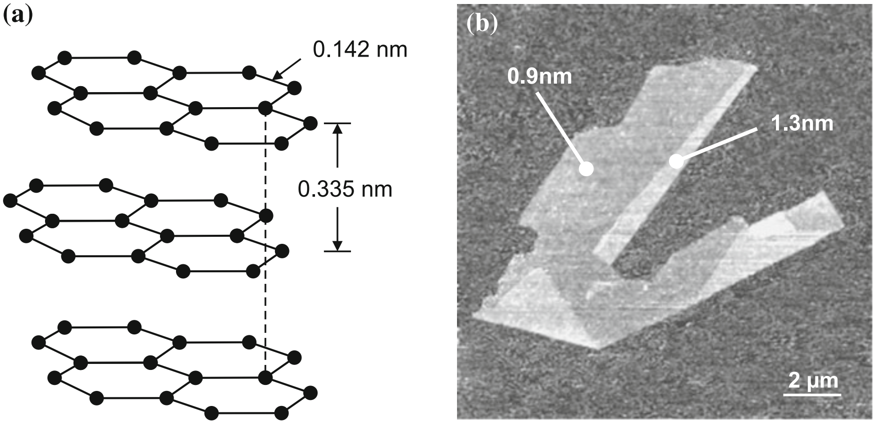

Fig. 18.2 (**a**) Schematic layer structure of graphite with bond length and layer distance labelled. (**b**) AFM image of graphene on oxidized silicon. The height of two areas relative to the background is labelled. Adapted from [1288]

around the Fermi energy at the K point (Fig. 18.4a). This point is also called Dirac point. The important bands close to the Fermi level stem from the π-orbitals. The linear dispersion around the K point is similar to that of relativistic particles without rest mass. The electrons in graphene are of course not really massless, their velocity (6.31) being $v = c_* \approx 10^6$ m/s, about 300 times smaller than the speed of light [1290, 1291].

In the simplest tight-binding approximation, the band structure is given as

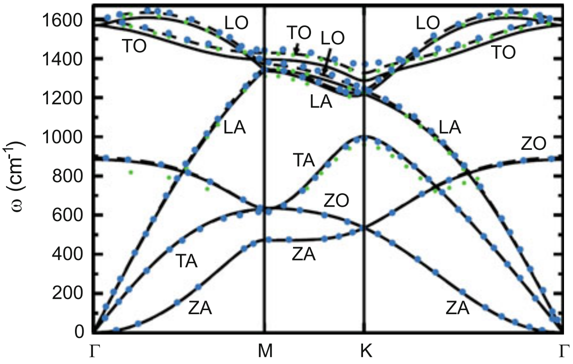

Fig. 18.3 Phonon dispersion in graphene. *Symbols* are experimental data from various methods. *Dashed lines* is DFT-LDA theory, *solid lines* GGA. Adapted from [1289]

$$E(\mathbf{k}) = \pm T \sqrt{1 + 4\cos\left(\frac{\sqrt{3}a\,k_y}{2}\right)\cos\left(\frac{a\,k_x}{2}\right) + 4\cos^2\left(\frac{a\,k_x}{2}\right)}, \tag{18.2}$$

where a is the lattice constant and $T \approx 3\,\mathrm{eV}$ is the next-neighbor hopping energy [1292]. In the meantime more elaborate tight-binding schemes have been reported [1293, 1294] as shown in Fig. 18.4b. The two-dimensional band structure is visualized in Fig. 18.4c. Such band structure has been directly confirmed experimentally [1295] as shown in Fig. 18.5a–e. The distortion of the band structure with increasing electron concentration (Fig. 18.5e–h) from the conical bands is due to strong electron–electron, electron–phonon, and electron–plasmon coupling effects [1295].

The band structure of FLG has been theoretically analysed in [1296]. For bilayers experimental data on the band structure can be found in [1297]. Subtle differences exist for different stacking orders of the graphene sheets. Bulk graphite shows a semi-metallic behavior with a band overlap of about 41 meV. For more than ten graphene layers the difference with the band overlap in bulk graphite is less than 10 %.

18.1.3 Electrical Properties

The Shubnikov-de Haas (SdH) oscillations from a graphene sheet exhibit a behavior [1291]

$$\frac{1}{\Delta B} = \frac{4e}{h}\,\frac{1}{n_\mathrm{S}}, \tag{18.3}$$

which corresponds to (13.38) for a two-dimensional electron system and a spin- and valley-degeneracy[1] of two. The cyclotron mass has been determined from the

---

[1] Each of the six valleys at the K points is shared by three Brillouin zones.

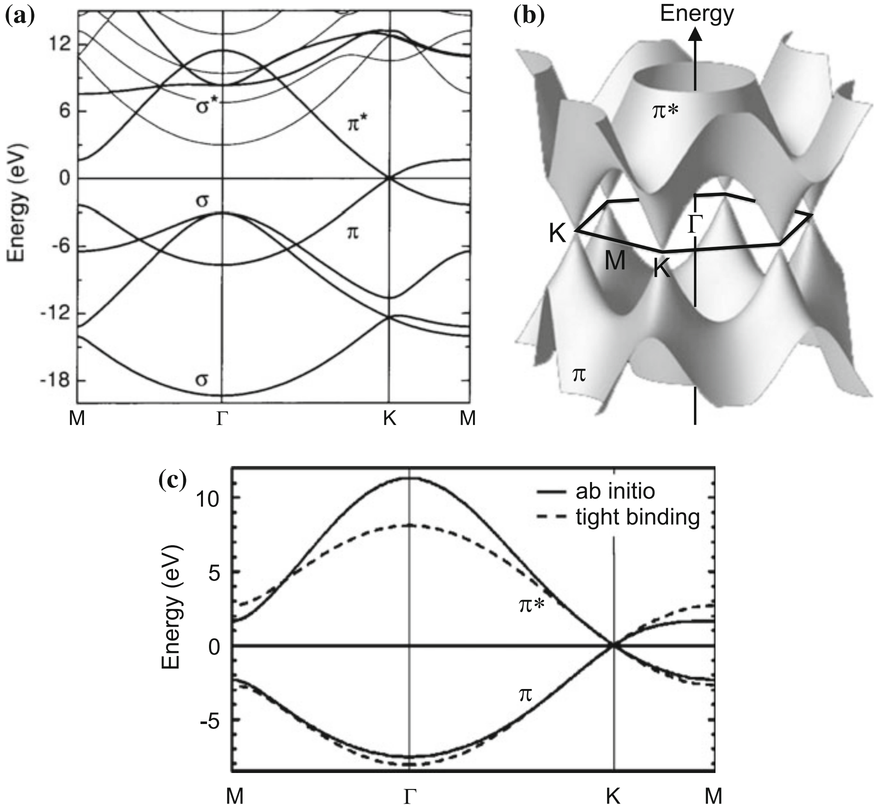

Fig. 18.4 (**a**) Band structure of graphene from first principles. (**b**) Three-dimensional representation $E(k_x, k_y)$ of the π-bands of graphene. (**c**) Band structure of graphene with only π-bands shown, *solid lines* are ab-initio calculation, *dashed lines* are calculated with tight-binding approximation. Adapted from [1294]

temperature dependence of the SdH oscillations to be proportional[2] to $\sqrt{n}$ (Fig. 18.6). The cyclotron mass is generally related [1298] to the area $S(E) = \pi k^2$ in k-space of the orbits at the Fermi energy via

$$m_\mathrm{c} = \frac{\hbar^2}{2\pi} \frac{\partial S(E)}{\partial E} \tag{18.4}$$

With the linear dispersion (18.1) we can write (18.4) as

$$m_\mathrm{c} = \frac{\hbar^2}{2\pi} \frac{2\pi\, E}{\hbar^2\, c_*^2} = \frac{E}{c_*^2}. \tag{18.5}$$

---

[2] In a parabolic dispersion as in (13.37), the cyclotron mass is independent of n.

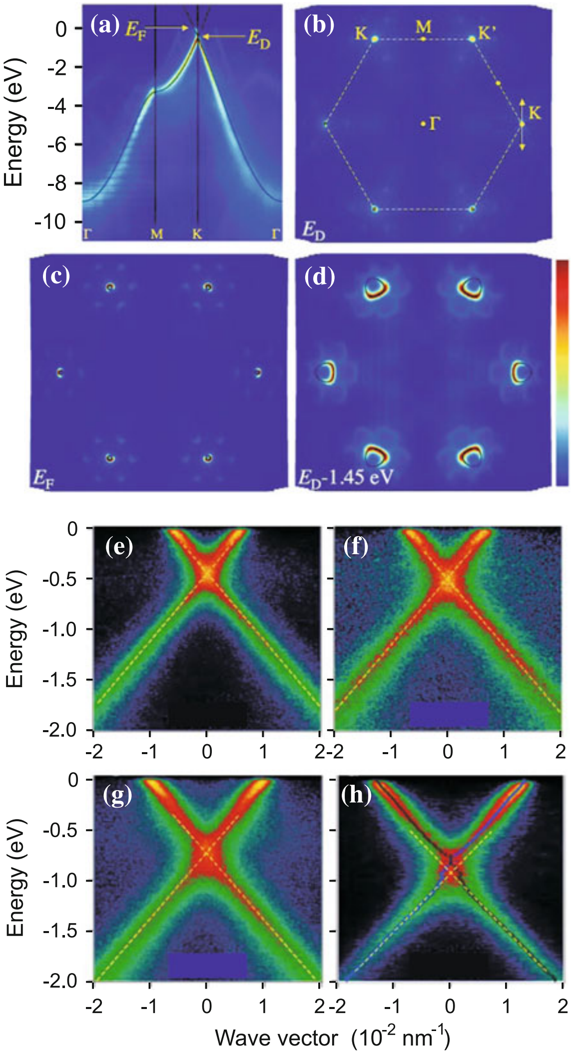

Fig. 18.5 Experimental bandstructure of graphene (on (0001) 6H-SiC) as determined from ARPES. (**a**) Energy distribution of states as a function of momentum along principal directions in the Brillouin zone. The single-orbital tight-binding model (18.2) with $T = 2.82\,\mathrm{eV}$ is shown as *solid lines*. The Fermi level is shifted by 0.435 eV due to doping. (**b**) Constant energy map of the states at binding energy corresponding to the Dirac energy E_D; the boundary of the Brillouin Zone boundary is superimposed as *dashed line*. The arrow at the K point indicates the directions over which the data in (**e**–**h**) were acquired. (**c**, **d**) Constant energy maps at the Fermi energy ($E_F = E_D + 0.45\,\mathrm{eV}$) and $E_D - 1.5\,\mathrm{eV}$, respectively. (**e**–**h**) Experimental energy bands along the line through the K point parallel to Γ–M direction as indicated in (**b**). The *dashed lines* are an extrapolation of the lower bands below the Dirac crossing energy, which are observed not to pass through the upper bands (above E_D), suggesting the kinked shape of the bands around E_D. The sheet electron density is $n_S = 1.1$, 1.5, 3.7, and $5.6 \times 10^{13}\,\mathrm{cm}^{-2}$ for (**e**)–(**h**), respectively, due to increased doping upon potassium adsorption. Adapted from [1295]

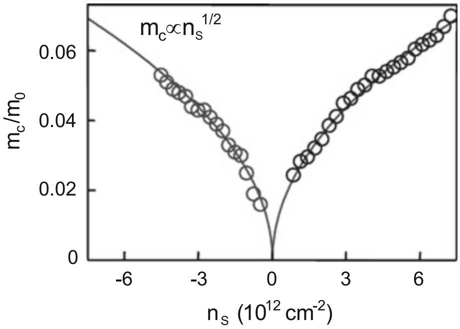

Fig. 18.6 Cyclotron mass in graphene as a function of the sheet electron concentration n_S (negative values relate to hole concentration, $E_F < E_D$). Adapted from [1291]

For the linear energy dispersion (18.1) the number of states up to energy E_F is (with a degeneracy of 4)

$$N(E_F) = 4\,\frac{\pi\,k_F^2}{(2\pi/L)^2} = A\,\frac{4\pi\,E_F^2}{h^2\,c_*^2}, \tag{18.6}$$

where A is the system area. Therefore we have (at low temperature) with (18.5)

$$n_S = \frac{4\pi}{h^2}\,\frac{E_F^2}{c_*^2} \propto m_c^2, \tag{18.7}$$

as determined experimentally. Therefore the behavior of the SdH oscillations confirms the linear dispersion relation. The experimental value for the velocity is $c_* \approx 10^6$ m/s. From (18.7) the density of states (per area and energy) around the Dirac point increases linearly with energy,

$$D(E) = \frac{8\pi}{h^2\,c_*^2}\,E. \tag{18.8}$$

The carrier density in a graphene sheet can be controlled via the field effect. The graphene is positioned on an insulator/semiconductor structure, typically SiO_2/Si (cf. Sect. 21.3). The carrier density is then related to the applied (gate) voltage V_g via (21.89) and (21.91), i.e.

$$n_S = \frac{\epsilon_i\,V_g}{e\,d}, \tag{18.9}$$

where d is the thickness of the insulator and ϵ_i its dielectric constant. By applying positive (negative) bias electron (holes) can be induced in the sheet. The electron and hole densities depend on the Fermi energies[3]

---

[3] Here we assume the linear dispersion for all thermally populated states.

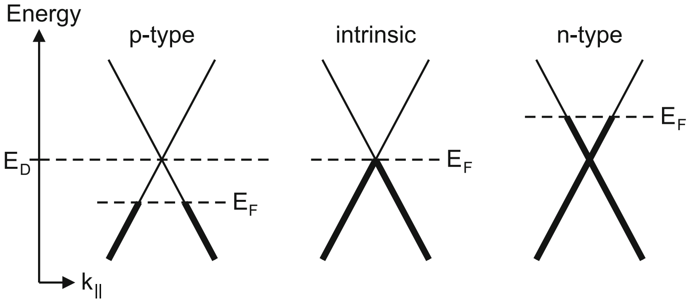

Fig. 18.7 Band structure of graphene with various positions of the Fermi energy E_F in relation to the Dirac energy E_D. States occupied with electrons are shown with in *bold*

$$n_\mathrm{S} = \frac{8\pi}{h^2\, c_*^2} \int_{E_\mathrm{D}}^{\infty} \frac{E - E_\mathrm{D}}{1 + \exp\left[(E - E_\mathrm{F})/kT\right]}\, \mathrm{d}E \tag{18.10a}$$

$$p_\mathrm{S} = \frac{8\pi}{h^2\, c_*^2} \int_{-\infty}^{E_\mathrm{D}} \frac{-(E - E_\mathrm{D})}{1 + \exp\left[-(E - E_\mathrm{F})/kT\right]}\, \mathrm{d}E \tag{18.10b}$$

as visualized in Fig. 18.7. These relations cannot be inverted to obtain $E_\mathrm{F}(n, p)$ analytically. The total charge carrier density is $\rho_\mathrm{S} = e(p_\mathrm{S} - n_\mathrm{S})$.

The Hall effect (Fig. 18.8) shows the expected ambipolar dependence according to (13.16) which takes the form

$$R_\mathrm{H} = \frac{1}{e}\, \frac{p_\mathrm{S} - n_\mathrm{S}}{(n_\mathrm{S} + p_\mathrm{S})^2} \tag{18.11}$$

for equal electron and hole mobilities.[4]

From Hall effect measurements the mobility has been determined to be about $10^4\,\mathrm{cm^2/Vs}$, independent of temperature between 10 and 100 K, and the same for electrons and holes. This value, however, is much smaller than the in-plane mobility of about $10^6\,\mathrm{cm^2/Vs}$ at 4.2 K in high quality samples of highly ordered pyrolithic graphite (HOPG) [1299]. In suspended graphene a mobility of $2.3 \times 10^5\,\mathrm{cm^2/Vs}$ has been found, limited by finite sample size [1300]. Thus in graphene layers on a solid surface extrinsic effects such as charge traps, interfacial phonons, ripples or fabrication residue seem to limit the carrier mobility.

The QHE has been observed in graphene [1291], reportedly up at room temperature [1301]. The plateaus $(4e^2/h)(n + 1/2)$ correspond to unusual half-integer filling, the first plateau occurring at $2e^2/h$, as has been also suggested from theory, and related to the 'pseudospin'. Another consequence of the Dirac-like behavior of the fermions in graphene is the presence of finite maximum resistiv-

---

[4] Including sign, $\mu_\mathrm{h} = -\mu_\mathrm{e}$. For $T = 0$ and $E_\mathrm{F} = E_\mathrm{D}$, $n_\mathrm{S} = p_\mathrm{S} = 0$ and thus $1/R_\mathrm{H}$ should be zero. For finite temperatures there is always $n_\mathrm{S} > 0$ and $p_\mathrm{S} > 0$, even for $E_\mathrm{F} = E_\mathrm{D}$. Thus $1/R_\mathrm{H} \propto 1/(p_\mathrm{S} - n_\mathrm{S})$ diverges at $\rho_\mathrm{S} = e(p_\mathrm{S} - n_\mathrm{S}) = 0$ with a change of sign.

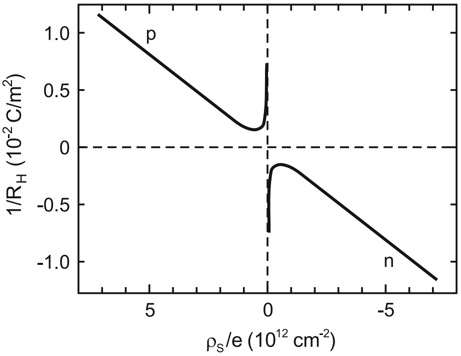

Fig. 18.8 Hall coefficient ($T = 10\,\mathrm{K}$) for a graphene sheet as a function of the free carrier sheet density $\rho_S/e = p_S - n_S$ (positive values indicate p-type). Data shown as *solid lines* from [1291]

ity $\rho_{\max} = h/4e^2 = 6.45\,\mathrm{k}\Omega$ even at low temperature and $E_F = E_D$. It is due to the fact that localization effects, leading to insulating behavior, are strongly suppressed. Then each carrier keeps a mean free path in the order of its Fermi wavelength.

The Klein paradox [1302, 1303], the efficient tunneling of Dirac particles through high and thick barriers seems accessible in transport experiments with graphene [1304].

18.1.4 Other Two-Dimensional Crystals

Two-dimensional crystals have been reported also for other materials such as BN, MoS_2, $NbSe_2$, $Bi_2Sr_2CaCu_2O_x$ [1286] or ZnO [1305]. The phonon spectra of graphene, BN- and BC_2N-sheets are compared in Fig. 18.9. The spectrum of BC_2N is similar to the superposition of the C and BN spectra [1306].

18.2 Carbon Nanotubes

18.2.1 Structure

A carbon nanotube (CNT) is a part of a graphene sheet rolled up to form a cylinder. They were first described as multi-walled nanotubes by Iijima [1307] in 1991 (Fig. 18.10b) and in their single-walled form (Fig. 18.10a) in 1993 [1308]. Reviews can be found in [1293, 1309].

The chirality and diameter of a nanotube are uniquely described by the chiral vector

$$\mathbf{c}_h = n_1\,\mathbf{a}_1 + n_2\,\mathbf{a}_2 \equiv (n_1, n_2), \tag{18.12}$$

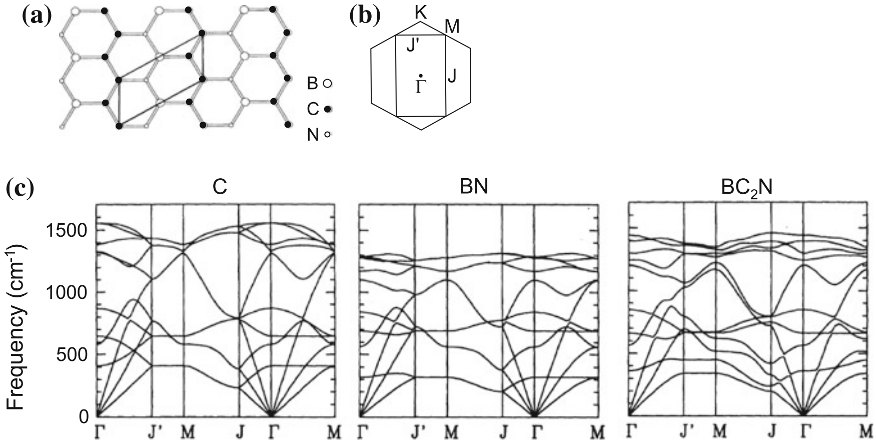

Fig. 18.9 (**a**) Crystal structure of BC_2N. (**b**) Brillouin zone of BC_2N (*rectangle*) and C, BN (*hexagon*). (**c**) Phonon dispersion of graphene (C) and BN- and BC_2N-sheets. Adapted from [1306]

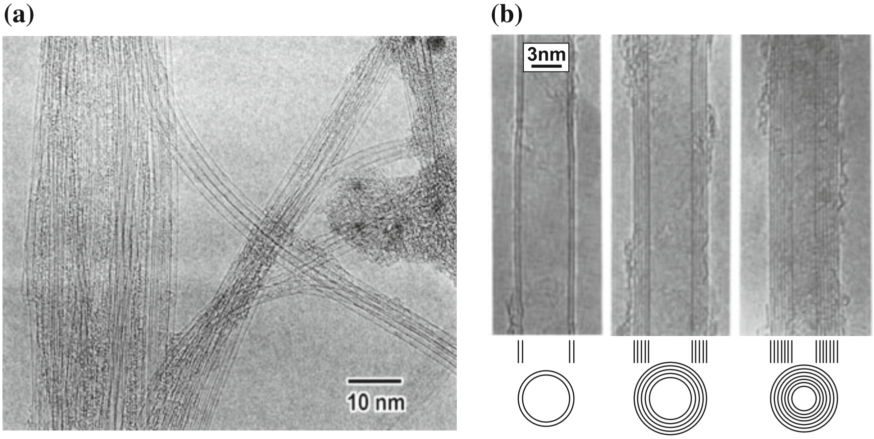

Fig. 18.10 (**a**) TEM image of single-walled carbon nanotubes (SWNT). (**b**) TEM images of various multi-walled carbon nanotubes (MWNT). Adapted from [1307]

where $\mathbf{a}_1$ and $\mathbf{a}_2$ are the unit vectors of the graphene sheet. The chiral vector denotes two crystallographic equivalent sites which are brought together along the circumference of the nanotube. The possible vectors are visualized in Fig. 18.1 for $-30° \leq \theta \leq 0°$. The fiber diameter is given by

$$d = \frac{|\mathbf{c}_\mathrm{h}|}{\pi} = \frac{a}{\pi}\left(n_1^2 + n_1 n_2 + n_2^2\right), \tag{18.13}$$

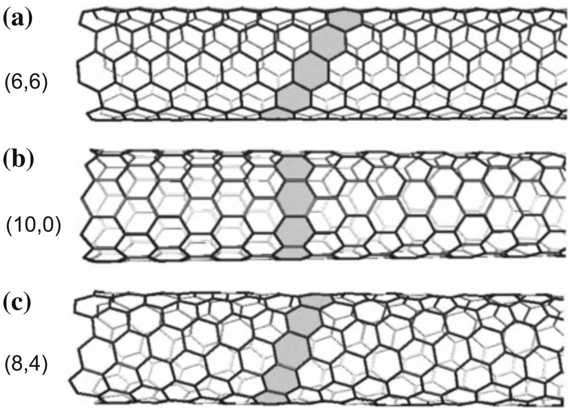

Fig. 18.11 Structure of different types of carbon nanotubes that have similar diameter of 0.8 nm. (**a**) Armchair (6,6), (**b**) zigzag (8,0) and (**c**) chiral symmetry. Adapted from [1309]

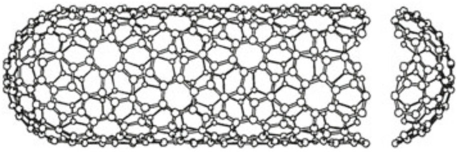

Fig. 18.12 A chiral nanotube (chiral vector is (10,5), $\theta = -19.11°$) with hemispherical caps at both ends based on an icosahedral C_{140} fullerene. The tube diameter is 1.036 nm. Adapted from [1311]

with the graphene lattice constant $a = \sqrt{3}\, d_{\mathrm{C-C}} = 0.246\,\mathrm{nm}$. Ab-initio calculations show that the diameter becomes a function of the chiral angle below 0.8 nm; deviations from (18.13) are below 2 % for tube diameters $d > 0.5\,\mathrm{nm}$ [1310]. The $(n, 0)$ tubes ($\theta = 0$) are termed 'zig-zag' and an example is depicted in Fig. 18.11b. Nanotubes with $\theta = \pm\,\pi/6$, i.e. of the (n, n) (and $(2n, -n)$) type, are called 'armchair'. All others are termed 'chiral'.

The extension along the wire axis is large compared to the diameter. The tip of a nanotube is part of a buckminster-fullerene type molecule (Fig. 18.12). When the nanotube if formed by rolling a single sheet of graphene (SLG), a single-walled nanotube (SWNT) is formed. A FLG sheet creates a multi-walled nanotube (MWNT). For small number of layers they are called double-walled, triple-walled and so forth.

The mechanical strength of carbon nanotubes is very large. For SWNT Young's moduli of 10^3 GPa have been found experimentally [1312] in agreement with theoretical predictions [1313].

18.2.2 Band Structure

In carbon nanotubes there is some mixing of the $\pi(2p_z)$ and $\sigma(2s$ and $2p_z)$ carbon orbitals due to the radial curvature. This mixing is, however, small and can

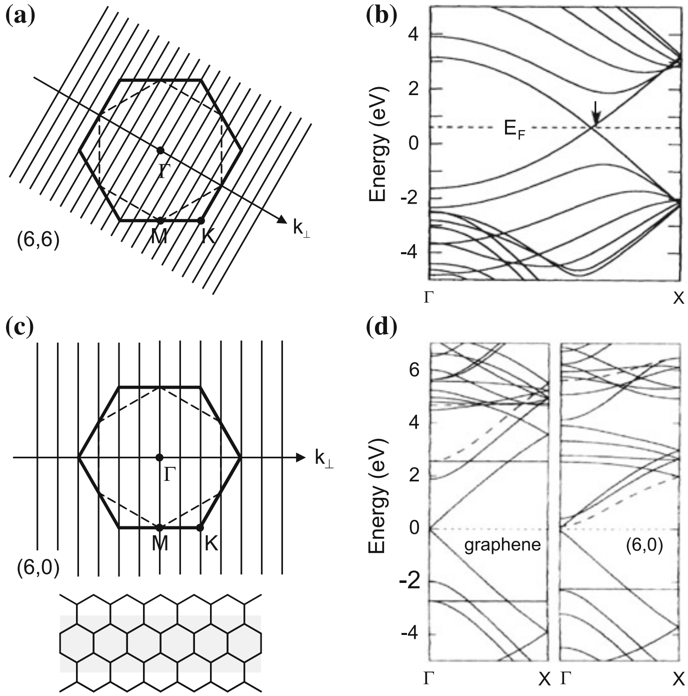

Fig. 18.13 (**a**) Brillouin zone of the graphene lattice (*bold line*) and allowed k-values for a (6,6) armchair nanotube. (**b**) Band structure of a (6,6) carbon nanotube. Adapted from [1315]. (**c**) Brillouin zone of the graphene lattice (*bold line*) and allowed k-values for a (6,0) zig-zag carbon nanotube. In the *lower part* the real space structure is visualized. (**d**) Band structure of graphene (*left*) and a (6,6) nanotube (*right*). Adapted from [1316]

be neglected near the Fermi level [1314]. The band structure of a nanotube is mainly determined by zone-folding of the graphene band structure. The vector along the (infinitely extended) wire k_z is continuous. The vector $k_\perp$ around the nanotube is discrete with the periodic boundary condition

$$\mathbf{c}_\mathrm{h} \cdot \mathbf{g}_\perp = 2\pi\, m, \tag{18.14}$$

where m is an integer. The distance of allowed $k_\perp$-values is (5.5)

$$\varDelta k_\perp = \frac{2\pi}{\pi\, d} = \frac{2}{d}. \tag{18.15}$$

The character of the nanotube band structure depends on how the allowed k-values lie relative to the graphene Brillouin zone and its band structure. This is visualized in Fig. 18.13. For the case of an armchair tube (n, n), as shown in Fig. 18.13a, the K-point of the graphene band structure always lies on an allowed k-point. Therefore,

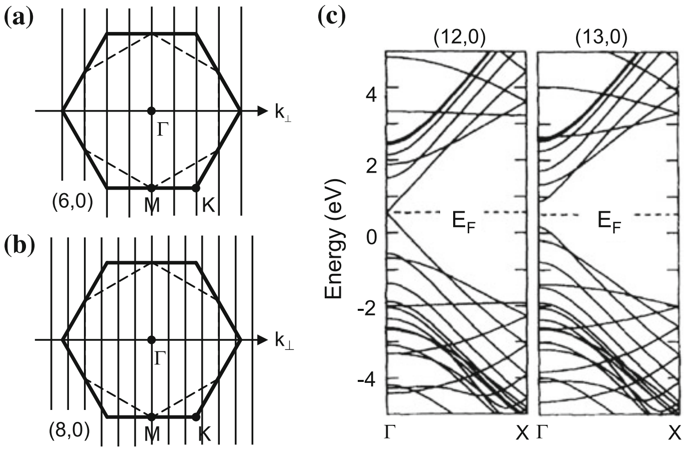

Fig. 18.14 (**a**, **b**) Brillouin zone of the graphene lattice (*bold line*) and allowed k-values for a (**a**) (6,0) and a (**b**) (8,0) zig-zag nanotube. (**c**) Band structures of a (12,0) metallic and (13,0) semiconducting armchair carbon nanotube. Adapted from [1315]

the nanotube is metallic, i.e. zero-gap, as seen in the bandstructure in Fig. 18.13b. The Dirac point is between Γ and X. For a zig-zag nanotube, the k-space is shown in Fig. 18.13c for a (6, 0) nanotube. The corresponding band structure for a (6, 0) nanotube is also metallic (Fig. 18.13d) with the Dirac point at the Γ point.

In Fig. 18.14c the band structure of another metallic (12, 0) zig-zag nanotube is shown. However, only for $(3m, 0)$ the K-point is on an allowed state and thus the tube metallic. For the other cases, as shown for the k-space of a (8, 0) nanotube in Fig. 18.14b, this is not the case. The corresponding band structure (Fig. 18.14c for (13, 0)) has a gap and thus the nanotube is a semiconductor. Generally, the condition for a nanotube to be metallic is with an integer m

$$n_1 - n_2 = 3\,m. \tag{18.16}$$

There are two semiconducting 'branches' with $\nu = (n_1 - n_2) \bmod 3 = \pm 1$. The tubes with $\nu = +1$ have a small band gap, those with $\nu = -1$ have a larger band gap.

The density of states is a series of one-dimensional DOS, proportional to $\sqrt{E}$ (6.75). It is compared in Fig. 18.15 for a metallic and a semiconducting nanotube. Within 1 eV from the Fermi energy the DOS can be expressed in an universal term [1317].

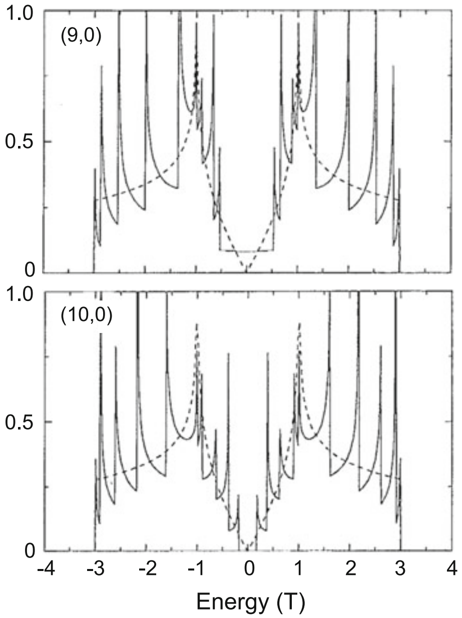

Fig. 18.15 Density of states for a (9,0) metallic and (10,0) semiconducting zig-zag carbon nanotube within the tight-binding approximation (18.2). The energy scale is given in units of the tight-binding parameter $T \approx 3\,\mathrm{eV}$. The *dashed lines* are the DOS of graphene. Adapted from [1311]

18.2.3 Optical Properties

Optical transitions occur with high probability between the van-Hove singularities of the DOS. The theoretical absorption spectrum of a (10,0) nanotube is shown in Fig. 18.16.

In an ensemble of nanotubes various types and sizes occur. The transition energies of all possible nanotubes sorted by diameter are assembled in the Kataura plot (Fig. 18.17a). Experimental data are shown in Fig. 18.17b. The two branches of semiconducting nanotubes $\nu = \pm 1$ yield different transition energies. The overall dependence of the transition energy follows a $1/d$-law.

18.2.4 Other Anorganic Nanotubes

Structures similar to carbon nanotubes have been reported for BN [1322, 1323]. A boron nitride nanotube is a cylindrically rolled part of a BN sheet. BN tubes are always semiconducting (Fig. 18.18) and have a band gap beyond 5 eV similar to hexagonal BN which is mostly independent on chirality and diameter [1324].

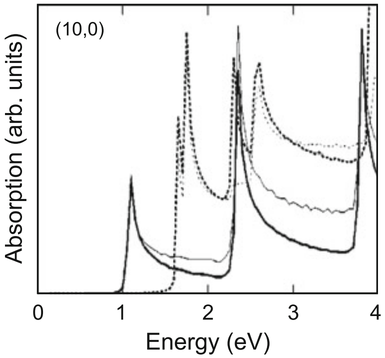

Fig. 18.16 Calculated absorption spectra for a (semiconducting) (10,0) carbon nanotube for parallel (*solid line*) and perpendicular (*dotted line*) polarization. The *thick* (*thin*) *lines* are calculated with (without) the matrix element included. Adapted from [1318]

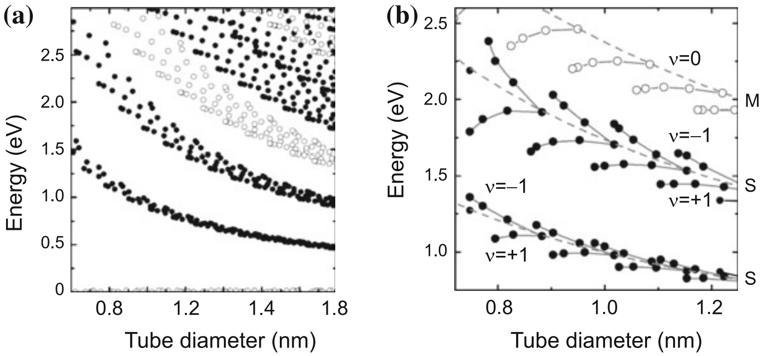

Fig. 18.17 (**a**) Theoretical transition energies of semiconducting (*filled symbols*) and metallic (*open symbols*) carbon nanotubes as a function of tube diameter (Kataura plot). Energies are calculated from van-Hove singularities in the JDOS within the third-order tight-binding approximation [1294]. (**b**) Experimental Kataura plot for the first two semiconducting (S, *closed symbols*) and the first metallic (M, *open symbols*) transition. *Dashed lines* connect the (near-to) armchair tubes; *full lines* connect tubes in a branch, $\nu = (n_1 - n_2) \bmod 3$. Data from photoluminescence [1319] and resonant Raman scattering [1320]. Adapted from [1321]

Thus, while carbon nanotubes appear black since they absorb within 0–4 eV, BN is transparent (or white if scattering). For high energies larger than 10 eV C and BN tubes are quite similar since they are isoelectronic and the high-lying unoccupied states are less sensitive to the difference in the nuclear charges than the states at and below the Fermi energy [1325].

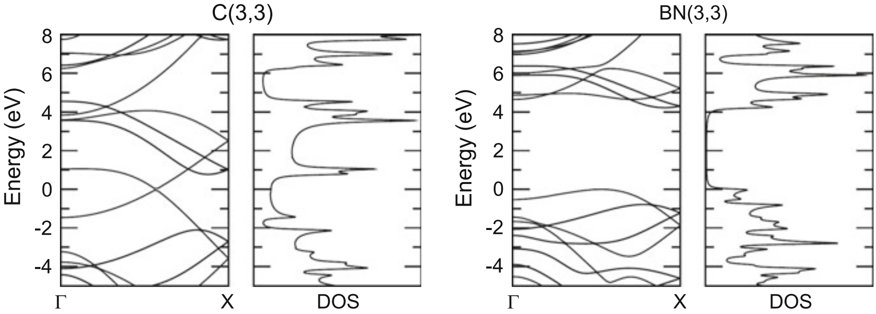

Fig. 18.18 Band structure and density of states (DOS) of C(3,3) and BN(3,3) nanotubes, calculated with DFT-LDA. Adapted from [1325]